JOURNAL OF COMPUTATIONAL PHYSICS 65, 386–409 (1986)

About the Coupling of Turbulence Closure Models with Averaged Navier–Stokes Equations

D. VANDROMME

Université des Sciences et Techniques de Lille,
U.E.R. de Mathématiques. Service de Mécanique, 59655 Villeneuve d'Ascq, Cédex, France

AND

H. HA MINH

Institut de Mécanique des Fluides de Toulouse, LA C.N.R.S. 005,
2, rue Camichel 31071 Toulouse, Cédex, France

Received June 13, 1984; revised October 16, 1985

The two-stage explicit–implicit method originally developped by MacCormack is extended to non-conservative equations. Different models using transport equations are presented. A special attention is paid to the conservation of total energy and to the correct treatment of the turbulent pressure terms. The implicit treatment of the source terms is detailed. The numerical method is applied to two turbulent flow calculations: (i) the 2-dimensional transonic flow over a bump, using either mixing length or two equation turbulence model; (ii) the supersonic compression–expansion ramp using a full Reynolds stress model as turbulence closure.

1. INTRODUCTION

During the past few years, significant progress has allowed to improve efficiency of computer solution algorithm for the viscous compressible Navier–Stokes equations. The implicit schemes brought up the concept of unconditional stability for unsteady or pseudo-unsteady numerical methods and it became possible to use high resolution grid for the treatment of viscous regions in high Reynolds number flows. The extension to turbulent flows was then possible by solving the Reynolds averaged Navier–Stokes equations and replacing the molecular diffusivity coefficients with their "effective" counterpart, including a locally defined turbulent viscosity. The major advantage of this algebraic-type turbulence model is to keep unchanged the structure of the motion equations and thus, most of the Navier–Stokes solvers could readily be extended to turbulent flows calculations. Unfortunately, although such a turbulence model does a fairly good job for equilibrium or weakly out-of-equilibrium flow prediction, the results are very poor when extra strain is applied to the turbulence field. As examples, we could mention curvature effects, strong shock waves, recirculation zones, or rotation effects. Attempts were made to improve complex flow predictions by introducing more sophisticated turbulence models. Following a first attempt with an explicit

0021-9991/86 $3.00

Navier–Stokes solver by Baldwin, MacCormack, and Deiwert et al [11], Viegas and Coakley [12] added one equation for the turbulent kinetic energy [13] in the hybrid method of MacCormack [14]. As the results with this model were not found significantly better, the method was extended to two-equation models in order to remove the uncertainty about the turbulent length scale determination. From that date, several two-equation turbulence models have been extensively used for complex flow calculations [15, 16, 17]. In the present work, the coupling which was not considered in the former references is examined for multi-equation turbulence models and new results obtained with a Reynolds stress (second order) turbulence closure are reported.

The compressible Navier–Stokes equations can be written in the following conservative form, for two-dimensional flows:

$$\frac{\partial U}{\partial t}+\frac{\partial F}{\partial x}+\frac{\partial G}{\partial y}=0 \tag{1}$$

where

$$U=\begin{bmatrix}\rho\\ \rho u\\ \rho v\\ \rho E\end{bmatrix} \tag{2}$$

$$F=\begin{bmatrix}\rho u\\ \rho u^2+\tau_{xx}\\ \rho uv+\tau_{xy}\\ (\rho E+\tau_{xx})\,u+\tau_{xy}v-K\dfrac{\partial T}{\partial x}\end{bmatrix} \tag{3a}$$

$$G=\begin{bmatrix}\rho v\\ \rho uv+\tau_{yx}\\ \rho v^2+\tau_{yy}\\ (\rho E+\tau_{yy})\,v+\tau_{yx}u-K\dfrac{\partial T}{\partial y}\end{bmatrix} \tag{3b}$$

and where

$$\begin{aligned}\tau_{xx}&=p-\lambda\left(\frac{\partial u}{\partial x}+\frac{\partial v}{\partial y}\right)-2\mu\frac{\partial u}{\partial x}\\ \tau_{yy}&=p-\lambda\left(\frac{\partial u}{\partial x}+\frac{\partial v}{\partial y}\right)-2\mu\frac{\partial v}{\partial y}\\ \tau_{xy}&=\tau_{yx}=-\mu\left(\frac{\partial u}{\partial y}+\frac{\partial v}{\partial x}\right)\end{aligned} \tag{3c}$$

with ρ the density, u and v the velocity components with respect to x and y components, λ and μ the viscosity coefficients, E the specific total energy, K the heat conduction coefficient and T the absolute gas temperature. Body forces and heat sources are not considered here although their existence would not bring any major change to the method. The pressure p is related to the specific internal energy according to the equation of state:

$$p = (\gamma - 1)\,\rho e \tag{4}$$

with

$$e = E - (u^2 + v^2)/2 \tag{5}$$

γ is the specific heat ratio.

The use of density-weighted average over the velocity field produces a set of equations applicable to turbulent flows. But then, the closure problem arises, for which the simplest solution is the use of a gradient flux approximation, similar to the Boussinesq proposal. Thus the turbulent viscosity can be determined from an algebraic relationship or from local turbulent quantities such as the turbulent kinetic energy, its dissipation rate or a turbulence length scale. The determination of these quantities requires the solution of non-conservative transport equations. For complex flows, it may be necessary to use a second-order closure which implies the solution of transport equations for every unknown statistical correlation emergent from second-order moment truncation. The introduction of these new equations adds constraints to the numerical method and occasionally reduces its generality.

In addition to the natural coupling due to the Reynolds stress terms (the closure problem), dependences appear in the total energy budget and in the pressure terms. A special treatment is needed for the source terms as well.

This paper sheds light on these new constraints in the framework of the MacCormack implicit predictor–corrector scheme [1], although these remarks can be applied to other numerical techniques which solve turbulence transport equations together with the compressible time averaged Navier-Stokes equations.

2. Turbulence Equations

When using density weighted averaging in conjunction with a two-equation turbulence model, the complete set of equations can be written as:

$$\frac{\partial U}{\partial t} + \frac{\partial F}{\partial x} + \frac{\partial G}{\partial y} = H \tag{6}$$

where

$$U = \begin{bmatrix} \bar{\rho} \\ \bar{\rho}\tilde{u} \\ \bar{\rho}\tilde{v} \\ \bar{\rho}\tilde{E} \\ \bar{\rho}k \\ \bar{\rho}\varepsilon \end{bmatrix} \tag{7}$$

$$F = \begin{bmatrix} \bar{\rho}\tilde{u} \\ \bar{\rho}\tilde{u}\tilde{u} + \tau_{xx} \\ \bar{\rho}\tilde{u}\tilde{v} + \tau_{xy} \\ (\bar{\rho}\tilde{E} + \tau_{xx})\,\tilde{u} + \tau_{xy}\tilde{v} - \left(\dfrac{\mu_l}{\mathscr{P}_r} + \dfrac{\mu_t}{\mathscr{P}_{rt}}\right) c_v \dfrac{\partial \tilde{T}}{\partial x} \\ \bar{\rho}\tilde{u}k + \sigma_{kx} \\ \bar{\rho}\tilde{u}\varepsilon + \sigma_{\varepsilon x} \end{bmatrix} \tag{8}$$

$$G = \begin{bmatrix} \bar{\rho}\tilde{v} \\ \bar{\rho}\tilde{u}\tilde{v} + \tau_{yx} \\ \bar{\rho}\tilde{v}^2 + \tau_{yy} \\ (\bar{\rho}\tilde{E} + \tau_{yy})\,\tilde{v} + \tau_{yx}\tilde{u} - \left(\dfrac{\mu_l}{\mathscr{P}_r} + \dfrac{\mu_t}{\mathscr{P}_{rt}}\right) c_v \dfrac{\partial \tilde{T}}{\partial y} \\ \bar{\rho}k + \sigma_{ky} \\ \bar{\rho}\varepsilon + \sigma_{\varepsilon y} \end{bmatrix} \tag{9}$$

$$H = \begin{bmatrix} 0 \\ 0 \\ 0 \\ 0 \\ S_k \\ S_\varepsilon \end{bmatrix}. \tag{10}$$

The diffusive fluxes are defined according to

$$\sigma_{\phi i} = -\left(\mu_l + \frac{\mu_t}{\sigma_\phi}\right)\frac{\partial \phi}{\partial x_i}. \tag{11}$$

The shear stresses are now written as

$$\tau_{ij} = \bar{p}\delta_{ij} - \mu_{\text{eff}}\left(\frac{\partial \tilde{u}_i}{\partial x_j} + \frac{\partial \tilde{u}_j}{\partial x_i}\right) + \frac{2}{3}\delta_{ij}\left(\mu_{\text{eff}}\frac{\partial \tilde{u}_k}{\partial x_k} + \bar{\rho}k\right) \tag{12}$$

where

$$\mu_{\text{eff}} = \mu_l + \mu_t \tag{13}$$

$$\mu_t = c_D f_\mu \bar{\rho}\frac{k^2}{\varepsilon} \tag{14}$$

f_μ is a turbulent Reynolds number dependent function which accounts for the wall vicinity effects. S_k and S_ε terms embody all the source terms which cannot be included in the divergence part of the equations for k and ε.

With a second-order closure model, the set of equations is written according to (1) with

$$U = \begin{bmatrix} \bar{\rho} \\ \bar{\rho}\tilde{u} \\ \bar{\rho}\tilde{v} \\ \bar{\rho}\tilde{E} \\ \bar{\rho}\widetilde{u''v''} \\ \bar{\rho}\varepsilon \\ \bar{\rho}\widetilde{u''^2} \\ \bar{\rho}\widetilde{v''^2} \\ \bar{\rho}\widetilde{w''^2} \end{bmatrix} \tag{15}$$

$$F = \begin{bmatrix} \bar{\rho}\tilde{u} \\ \bar{\rho}\tilde{u}^2 + \tau_{xx} \\ \bar{\rho}\tilde{u}\tilde{v} + \tau_{xy} \\ (\bar{\rho}\tilde{E} + \tau_{xx})\,\tilde{u} + \tau_{xy}\tilde{v} - \left(\dfrac{\mu_l}{\mathscr{P}_r} + \dfrac{\mu_t}{\mathscr{P}_{rt}}\right) c_v \dfrac{\partial \tilde{T}}{\partial x} \\ \bar{\rho}\widetilde{u''v''}\tilde{u} \\ \bar{\rho}\varepsilon\tilde{u} \\ \bar{\rho}\widetilde{u''^2}\tilde{u} \\ \bar{\rho}\widetilde{v''^2}\tilde{u} \\ \bar{\rho}\widetilde{w''^2}\tilde{u} \end{bmatrix} \tag{16}$$

$$G = \begin{bmatrix} \bar{\rho}\tilde{v} \\ \bar{\rho}\tilde{u}\tilde{v} + \tau_{yx} \\ \bar{\rho}\tilde{v}^2 + \tau_{yy} \\ (\bar{\rho}\tilde{E} + \tau_{yy})\,\tilde{v} + \tau_{yx}\tilde{u} - \left(\dfrac{\mu_l}{\mathscr{P}_r} + \dfrac{\mu_t}{\mathscr{P}_{rt}}\right)\dfrac{\partial \tilde{T}}{\partial y} \\ \bar{\rho}\widetilde{u''v''}\tilde{v} \\ \bar{\rho}\tilde{\varepsilon}\tilde{v} \\ \bar{\rho}\widetilde{u''^2}\tilde{v} \\ \bar{\rho}\widetilde{v''^2}\tilde{v} \\ \bar{\rho}\widetilde{w''^2}\tilde{v} \end{bmatrix} \tag{17}$$

$$H = \begin{bmatrix} 0 \\ 0 \\ 0 \\ 0 \\ S_{\widetilde{u''v''}} \\ S_{\varepsilon} \\ S_{\widetilde{u''^2}} \\ S_{\widetilde{v''^2}} \\ S_{\widetilde{w''^2}} \end{bmatrix}. \tag{18}$$

The stresses with that type of model are

$$\tau_{ij} = \bar{p}\delta_{ij} + \bar{\rho}\widetilde{u_i'' u_j''} - \mu_l\left[\frac{\partial \tilde{u}_i}{\partial x_j} + \frac{\partial \tilde{u}_j}{\partial x_i} - \frac{2}{3}\delta_{ij}\frac{\partial \tilde{u}_k}{\partial x_k}\right]. \tag{19}$$

The S_ϕ terms are the sources of the transport equations for the turbulence quantities. In all the previous equations, the molecular viscosity fluctuations have been neglected. In fact, the detailed form of the modeled equations would show more terms than presented in Eqs. (15) to (19). Nevertheless, the structure of the equations is the same, and as the present paper is devoted only to the computational aspects of this effort to solve the Navier–Stokes equations, the reader is sent back to the references [2, 3, 4] for a detailed description of the turbulence modeling aspects of the problem.

3. The Coupling Problem

The instantaneous form of the total energy definition is

$$E = e + u_i^2/2 \tag{20}$$

with e standing for the internal energy of the fluid. In terms of mean and fluctuating components, this equation becomes, after time-averaging,

$$\tilde{E} = \tilde{e} + \tilde{u}_i^2/2 + k. \tag{21}$$

Therefore, when solving the Navier–Stokes equations, it appears clearly that the turbulent kinetic energy, k, must be known to determine the internal energy and the pressure field. For incompressible flow calculations, the energy budget is ignored and the turbulent motion is only superimposed on the mean. The coupling appears only through the turbulent friction which is added to the viscous effects. However, for compressible flows calculations, all energetic exchanges between the different scale motions must be considered to satisfy the energy conservation.

The Boussinesq approximation for the Reynolds stress is written as

$$-\bar{\rho}\,\widetilde{u_i'' u_j''} = \mu_t \left(\frac{\partial \tilde{u}_i}{\partial x_j} + \frac{\partial \tilde{u}_j}{\partial x_i} - \frac{2}{3}\,\delta_{ij} \frac{\partial \tilde{u}_k}{\partial x_k} \right) - \frac{2}{3}\,\delta_{ij}\bar{\rho}k \tag{22}$$

where the presence of the turbulent kinetic energy term allows the contracted index form. This feature appears in the momentum and total energy equations where a turbulent normal stress is added to the mean pressure term. Therefore a so-called effective pressure can be defined in the following way:

$$p^* = \bar{p} + \tfrac{2}{3}\bar{\rho}k. \tag{23}$$

In fact, this scalar turbulent contribution to the pressure field is only an approximation which neglects the anisotropic nature of the Reynolds stress tensor. Such an approximation does not exist formally with a second-order closure turbulence model. The normal stresses appear explicitly in the momentum and total energy equations. The corresponding effective pressure is not isotropic any longer but depends also on the distribution of the turbulent energy on its three normal components. In the i-momentum equation the effective pressure will be

$$p_i^* = \bar{p} + \bar{\rho}\widetilde{u_i''^2}. \tag{24}$$

Nevertheless, the concept of anisotropic effective pressure is difficult to handle, especially when relating to the temperature field. Therefore the scalar contribution is assumed for computational convenience. The addition to the static pressure is motivated by the equilibrium definition from the kinetic theory of gases, where the turbulent pressure is approximated with the average value $\frac{2}{3}\bar{\rho}k$.

In some sense, the introduction of this effective pressure is analogous to the appearance of bulk viscosity in flows with translational non-equilibrium [5], for which a thermodynamic or equilibrium pressure can be defined in terms of $\bar{\rho}$ and $\tilde{T}$, which themselves have unambigous physical definitions. As in the bulk viscosity

situation, two different mean temperatures can be distinguished, the static and the effective temperatures $\tilde{T}$ an T^*:

$$\left.\begin{aligned} \bar{p} &= \bar{\rho} R \tilde{T} \\ p^* &= \bar{\rho} R T^* \end{aligned}\right\} \rightarrow T^* - \tilde{T} = \frac{2k}{3R}. \tag{25}$$

Then, it is easy to show that the relative difference in temperature is very small (less than 1%). Also when looking at the definition of the effective pressure, the turbulent contribution is small compared to the static pressure; nevertheless in highly sheared regions, the gradient of k can be twice as large as the conventional pressure gradient.

4. The Numerical Treatment of the Equations

4.1. *Diagonalization of the Jacobian Matrices*

In order to avoid the classical stability limitations of explicit schemes, an implicit operator allows the use of large time steps. At each time step, the explicit increment is updated with the solution of a transport equation. That equation is obtained by taking the time derivative of the original vector equation [1].

$$A = \frac{\partial F}{\partial U}; \qquad B = \frac{\partial G}{\partial U}; \qquad C = \frac{\partial H}{\partial U} \tag{26}$$

we have

$$\left(I + \Delta t . \frac{\partial A .}{\partial x} + \Delta t \frac{\partial B .}{\partial y} - \Delta t . C \right) \delta U^{n+1} = \Delta U^n \tag{27}$$

where

$$\delta U^{n+1} = \Delta t \left(\frac{\partial U}{\partial t} \right)^{n+1}; \qquad \Delta U^n = \Delta t \left(\frac{\partial U}{\partial t} \right)^n. \tag{28}$$

The complete approximate factorization of this equation yields

$$\left(I + \Delta t \frac{A .}{x} \right) \left(I + \Delta t . \frac{\partial B .}{\partial y} \right) (I - \Delta t . C) \, \delta U^{n+1} = \Delta U^n. \tag{29}$$

The implicit part δU^{n+1} of the increment is calculated from the explicit part ΔU^n. To solve that equation for δU^{n+1}, it would be necessary to go through a block tridiagonal algorithm which is both memory and time consuming. To avoid this, an elegant and efficient method consists in diagonalizing the jacobian matrices. Then the solution is obtained only by inverting a lower or upper bidiagonal matrix [1].

In the following developments, it will be shown that the turbulence energy needs to be included in the diagonalization process. Then the specific treatment of the source terms will be explained and discussed.

In a first step, the viscous terms are set to zero. All these effects will be restored at a later stage in the algorithm. The diagonalization of the jacobian matrices corresponds to the transformation of the conventional conservative variables into nonconservative and then characteristic quantities. With a two-equation turbulence model, the first transformation of conservative into nonconservative variables is done with the matrix product:

$$\delta U_{\mathrm{nc}} = SX_1 \cdot \delta U_{\mathrm{c}}$$

$$\delta U_{\mathrm{c}} = \begin{bmatrix} \delta(\bar{\rho}) \\ \delta(\bar{\rho}u) \\ \delta(\bar{\rho}v) \\ \delta(\bar{\rho}E) \\ \delta(\bar{\rho}k) \\ \delta(\bar{\rho}\varepsilon) \end{bmatrix} \xrightarrow{SX_1} \delta U_{\mathrm{nc}} = \begin{bmatrix} \delta(\bar{\rho}) \\ \delta(\tilde{u}) \\ \delta(\tilde{v}) \\ \delta(p^*) \\ \delta(k) \\ \delta(\varepsilon) \end{bmatrix} \tag{30a}$$

where

$$SX_1 = \begin{bmatrix} 1 & 0 & 0 & 0 & 0 & 0 \\ -\dfrac{\tilde{u}}{\bar{\rho}} & \dfrac{1}{\bar{\rho}} & 0 & 0 & 0 & 0 \\ -\dfrac{\tilde{v}}{\bar{\rho}} & 0 & \dfrac{1}{\bar{\rho}} & 0 & 0 & 0 \\ \alpha\beta & -\beta\tilde{u} & -\beta\tilde{v} & \beta & -\beta & 0 \\ -\dfrac{k}{\bar{\rho}} & 0 & 0 & 0 & \dfrac{1}{\bar{\rho}} & 0 \\ -\dfrac{\varepsilon}{\bar{\rho}} & 0 & 0 & 0 & 0 & \dfrac{1}{\bar{\rho}} \end{bmatrix}. \tag{30b}$$

The transformation of nonconservative to characteristic variables follows as (for the x operator):

$$\delta U_{\mathrm{char}} = SX_2 \cdot \delta U_{\mathrm{nc}}$$

$$\delta U_{\mathrm{nc}} = \begin{bmatrix} \delta(\bar{\rho}) \\ \delta(\tilde{u}) \\ \delta(\tilde{v}) \\ \delta(p^*) \\ \delta(k) \\ \delta(\varepsilon) \end{bmatrix} \xrightarrow{SX_2} \delta U_{\mathrm{char}} = \begin{bmatrix} \delta(\bar{\rho}) - \dfrac{1}{c^{*2}}\delta(p^*) \\ \delta(p^*) + \bar{\rho}c^*\delta(\tilde{u}) \\ \delta(\tilde{v}) \\ \delta(p^*) - \bar{\rho}c^*\delta(\tilde{u}) \\ \delta(k) \\ \delta(\varepsilon) \end{bmatrix} \tag{31a}$$

where

$$SX_2 = \begin{bmatrix} 1 & 0 & 0 & \frac{1}{c^{*2}} & 0 & 0 \\ 0 & \tilde{\rho}c^* & 0 & 1 & 0 & 0 \\ 0 & 0 & 1 & 0 & 0 & 0 \\ 0 & -\tilde{\rho}c^* & 0 & 1 & 0 & 0 \\ 0 & 0 & 0 & 0 & 1 & 0 \\ 0 & 0 & 0 & 0 & 0 & 1 \end{bmatrix}. \tag{31b}$$

The direct transformation is made with the matrix product

$$SX = SX \cdot SX_1 \tag{32}$$

$$SX = \begin{bmatrix} 1 - \frac{\alpha\beta}{c^{*2}} & \frac{\beta\tilde{u}}{c^{*2}} & \frac{\beta\tilde{v}}{c^{*2}} & -\frac{\beta}{c^{*2}} & \boxed{\frac{\beta}{c^{*2}}} & 0 \\ -\tilde{u}c^* + \alpha\beta & c^* - \beta\tilde{u} & -\beta\tilde{u} & \beta & -\beta & 0 \\ -\frac{\tilde{v}}{\tilde{\rho}} & 0 & \frac{1}{\tilde{\rho}} & 0 & 0 & 0 \\ \tilde{u}c^* + \alpha\beta & -c^* - \beta\tilde{u} & -\beta\tilde{v} & \beta & -\beta & 0 \\ \boxed{-\frac{k}{\tilde{\rho}}} & 0 & 0 & 0 & \boxed{\frac{1}{\tilde{\rho}}} & 0 \\ \boxed{-\frac{\varepsilon}{\tilde{\rho}}} & 0 & 0 & 0 & 0 & \boxed{\frac{1}{\tilde{\rho}}} \end{bmatrix}.$$

Then it is straighforward to show that

$$SX^{-1} = \begin{bmatrix} 1 & \frac{1}{2c^{*2}} & 0 & \frac{1}{2c^{*2}} & 0 & 0 \\ \tilde{u} & \frac{\tilde{u}}{2c^{*2}} + \frac{1}{2c^*} & 0 & \frac{\tilde{u}}{2c^{*2}} - \frac{1}{2c^*} & 0 & 0 \\ \tilde{v} & \frac{\tilde{v}}{2c^{*2}} & \tilde{\rho} & \frac{\tilde{v}}{2c^{*2}} & 0 & 0 \\ \alpha\boxed{+k} & \frac{\alpha + \boxed{k}}{2c^{*2}} + \frac{\tilde{u}}{2c^*} + \frac{1}{2\beta} & \tilde{\rho}\tilde{v} & \frac{\alpha + \boxed{k}}{2c^{*2}} - \frac{\tilde{u}}{2c^*} + \frac{1}{2\beta} & \boxed{\tilde{\rho}} & 0 \\ \boxed{k} & \boxed{\frac{k}{2c^{*2}}} & 0 & \boxed{\frac{k}{2c^{*2}}} & \tilde{\rho} & 0 \\ \boxed{\varepsilon} & \boxed{\frac{\varepsilon}{2c^{*2}}} & 0 & \boxed{\frac{\varepsilon}{2c^{*2}}} & 0 & \tilde{\rho} \end{bmatrix}.$$

The transformed matrices SY and SY^{-1} for the y operator have a similar form and are not reproduced here. In SX and SX^{-1}, the dashed frames show the contributions of the new equations when added only to the original system. The solid frames show the result of the coupling between the equations due to the energy budget. The speed of sound c^*, which is used here must be interpreted as the effective speed defined previously.

Thus, the turbulence energy terms appear explicitly in the jacobian matrix.

$$A = \begin{bmatrix} 0 & 1 & 0 & 0 & 0 & 0 \\ \frac{\gamma-3}{2}\tilde{u}^2 + \frac{\beta\tilde{v}^2}{2} & (3-\gamma)\,\tilde{u} & -\beta\tilde{v} & \beta & -\beta & 0 \\ -\tilde{u}\tilde{v} & \tilde{v} & \tilde{u} & 0 & 0 & 0 \\ 2\beta\tilde{u}\alpha - \gamma\tilde{E}\tilde{u} + \boxed{\beta\tilde{u}k} & \gamma\tilde{E} - \beta\frac{3\tilde{u}^2+\tilde{v}^2}{2} & \boxed{-\beta k} & -\beta\tilde{u}\tilde{v} & \gamma\tilde{u} & \boxed{-\beta\tilde{u}} & 0 \\ \boxed{-\tilde{u}k} & \boxed{k} & 0 & 0 & \boxed{\tilde{u}} & 0 \\ \boxed{-\tilde{u}\varepsilon} & \boxed{\varepsilon} & 0 & 0 & 0 & \boxed{\tilde{u}} \end{bmatrix}$$

$$\beta = \gamma - 1; \qquad \alpha = (\tilde{u}^2 + \tilde{v}^2)/2.$$

It is easy to verify that the diagonal matrix is

$$\Lambda_A = \begin{bmatrix} \tilde{u} & 0 & 0 & 0 & 0 & 0 \\ 0 & \tilde{u}+c^* & 0 & 0 & 0 & 0 \\ 0 & 0 & \tilde{u} & 0 & 0 & 0 \\ 0 & 0 & 0 & \tilde{u}-c^* & 0 & 0 \\ 0 & 0 & 0 & 0 & \tilde{u} & 0 \\ 0 & 0 & 0 & 0 & 0 & \tilde{u} \end{bmatrix} \tag{33}$$

where

$$A = SX^{-1} \cdot \Lambda_A \cdot SX. \tag{34}$$

The restoration of the viscous effects is made as described in the original paper of MacCormack through a change of the eigenvalues [1].

With a second-order closure model, the turbulence energy is explicitly distributed on its three normal components. To illustrate this feature, only the jacobian matrix A is shown here, but the derivation method is similar for the transverse direction.

$$A = \begin{bmatrix}
0 & 1 & 0 & 0 & 0 & 0 & 0 & 0 & 0 \\
\frac{\gamma}{2}\tilde{u}^2 + \frac{\gamma-1}{2}\tilde{v}^2 & (3-\gamma)\tilde{u} & -\beta\tilde{v} & \beta & 0 & 0 & -\frac{\beta}{2} & -\frac{\beta}{2} & -\frac{\beta}{2} \\
-\tilde{u}\tilde{v} & \tilde{v} & \tilde{u} & 0 & 0 & 0 & 0 & 0 & 0 \\
2u\beta\alpha + \gamma E u + \beta\tilde{u}k & \gamma\tilde{E} - \frac{3\tilde{u}^2+\tilde{v}^2}{2} - \beta k & \beta\tilde{u}\tilde{v} & \gamma\tilde{u} & 0 & 0 & -\beta\frac{\tilde{u}}{2} & -\beta\frac{\tilde{u}}{2} & -\beta\frac{\tilde{u}}{2} \\
-\widetilde{u''v''}\tilde{u} & \widetilde{u''v''} & 0 & 0 & \tilde{u} & 0 & 0 & 0 & 0 \\
-\varepsilon\tilde{u} & \varepsilon & 0 & 0 & 0 & \tilde{u} & 0 & 0 & 0 \\
-\widetilde{u''^2}\tilde{u} & \widetilde{u''^2} & 0 & 0 & 0 & 0 & \tilde{u} & 0 & 0 \\
-\widetilde{v''^2}\tilde{u} & \widetilde{v''^2} & 0 & 0 & 0 & 0 & 0 & \tilde{u} & 0 \\
-\widetilde{w''^2}\tilde{u} & \widetilde{w''^2} & 0 & 0 & 0 & 0 & 0 & 0 & \tilde{u}
\end{bmatrix} \tag{35}$$

5. Implicit Treatment of the Source Terms

The implicit increment obeys the following approximate transport equation:

$$\left(I + \Delta t \frac{\partial A.}{\partial x}\right)\left(I + \Delta t \frac{\partial B.}{\partial y}\right)(I - \Delta t.C)\,\delta U^{n+1} = \Delta U^n. \tag{36}$$

The A and B matrices have been defined previously, assuming an inviscid character of the equations. Similarly the Jacobian matrix for the source terms is written as

$$\delta H = C.\delta U. \tag{37}$$

As the content of H is much more complex than for F and G, it is not possible to derive a analytical form for its jacobian matrix. To keep some generality for the expression of C, the structure of the H content is assumed unknown, and C is written as

$$C = \begin{bmatrix}
0 & 0 & 0 & 0 & 0 & 0 & 0 \\
0 & 0 & 0 & 0 & 0 & 0 & 0 \\
0 & 0 & 0 & 0 & 0 & 0 & 0 \\
0 & 0 & 0 & 0 & 0 & 0 & 0 \\
0 & 0 & 0 & 0 & 0 & \frac{S_k}{\bar{\rho}k} & 0 \\
0 & 0 & 0 & 0 & 0 & 0 & \frac{S_\varepsilon}{\bar{\rho}\varepsilon}
\end{bmatrix}.$$

with S_k and S_ε the respective sources of k and ε equations. Obviously, in a second-order closure turbulence framework, the matrix C has a higher dimension but is defined on the same principle. If we follow the inversion process, the explicit increment is modified first by the source matrix before being updated by the spatial derivative operators:

$$\left(I+\Delta t\frac{\partial B}{\partial y}\right)\left(I+\Delta t\frac{\partial A}{\partial x}\right)\delta U^{n+1}=\Delta U^n(I+\Delta t.\,|C|)^{-1}. \tag{38}$$

A different approach of this treatment avoids the third factorization. Then the source are grouped to the transverse spatial derivative term through the maximum eigenvalue [6]. In that case, the same maximum increment is applied to the whole set of nonconservative transport equations. A second alternative is being followed by Viegas [7]. This consists of simplifying part of the source terms (by elimination, for instance) to allow the derivation of an analytical form for the jacobian matrix. This approach tries to be more rigorous in the implicit approximation but seems usable only for simple two equation models. As far as second-order closure is concerned, in spite of already too numerous simplifications, the analytical form is not yet accessible. The lack of flexibility of this last method makes any specific work on the turbulence models themselves difficult.

6. Applications

6.1. *Transonic nozzle*

To illustrate the capacity of this numerical method to predict turbulent flows, a time dependant calculation is presented which converges on, a steady state solution. The 2-dimensional transonic flow which was submitted by Delery [8] to the 1981 Stanford conference is used as a test case.

Figures 1 to 5, extracted from the conference preparation notes, show the main

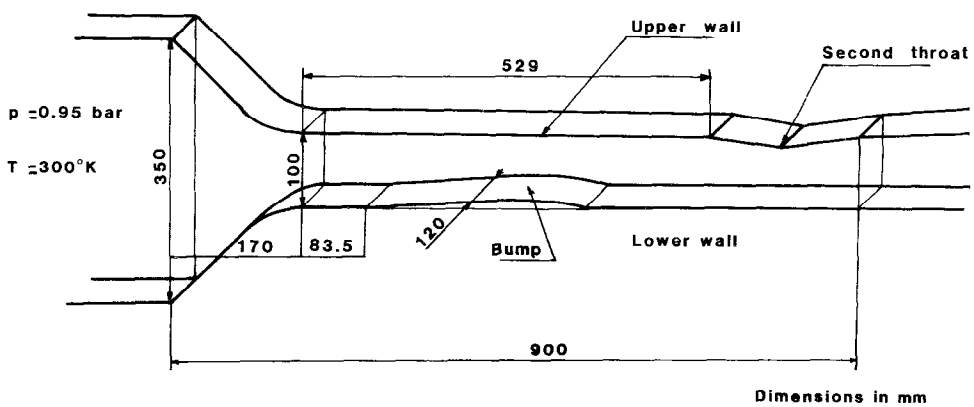

FIG. 1. Nozzle set-up.

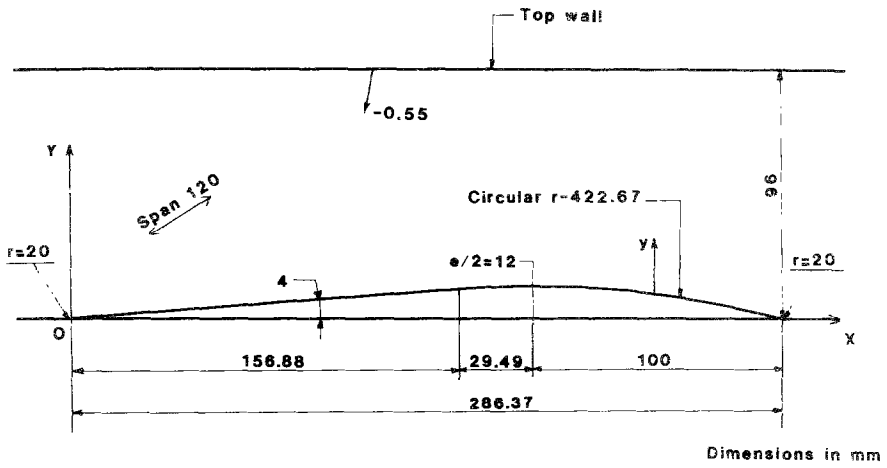

FIG. 2. Nozzle geometry.

features of the flow. In Fig. 1, the nozzle set-up is presented. A bump, for which the

asymptotic Mach number value (close to 1.4) is reached. The downstream pressure which is controlled by an adjustable second throat produces a normal shock wave above the bump trailing edge. The pressure gradient, induced by this shock wave is strong enough to create a boundary layer separation with an extended recirculation zone.

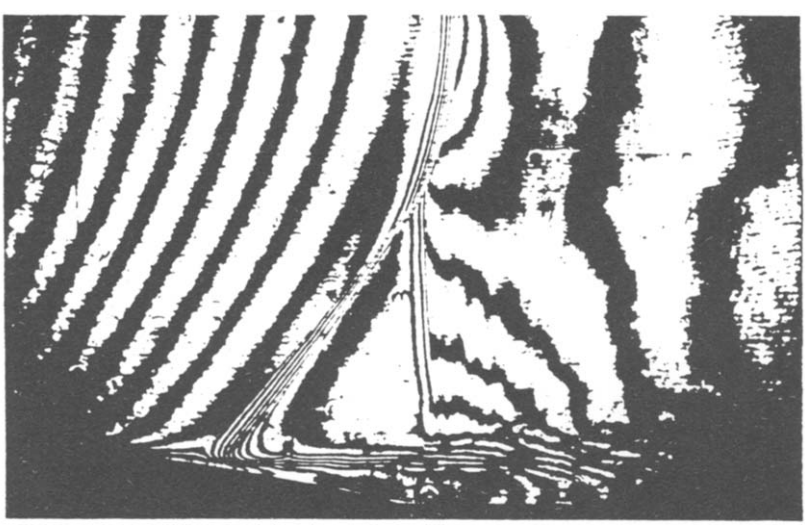

FIG. 3. Flow aspect.

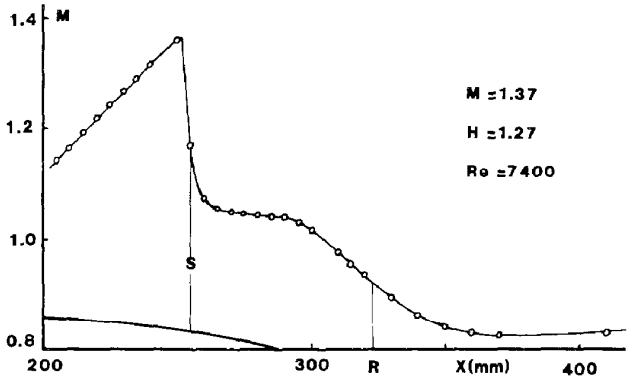

FIG. 4. Mach number distribution (from measured pressure).

This largge separation region produces an oblique shock C_1 issued from the separation point (Fig. 5). Downstream of C_1, the flow which is still supersonic, meets a quasi-normal second shock. The two shocks C_1 and C_2 join each other above the interaction zone to form an unique normal shock wave across the remaining part of the nozzle. The separated region corresponds to a plateau-like shape of the lower wall pressure curve (Fig. 4). The respective positions of the separation and reattachment points have been evaluated experimentally at 0.260m and 0.325m from the bump leading edge. The reservoir conditions are:

$$p_0 = 95000 N/\mathrm{m}^2 \qquad T_0 = 300^\circ\mathrm{K}$$

the boundary layer at the beginning of the interaction zone is characterized by

$$\text{Mach number} = 1.36 \qquad \delta = 0.005\mathrm{m}$$

$$\delta^* = 0.000518\mathrm{m} \qquad \theta = 0.000265\mathrm{m}$$

the momentum thickness Reynolds number is $\mathrm{Re}_\theta = 3800$.

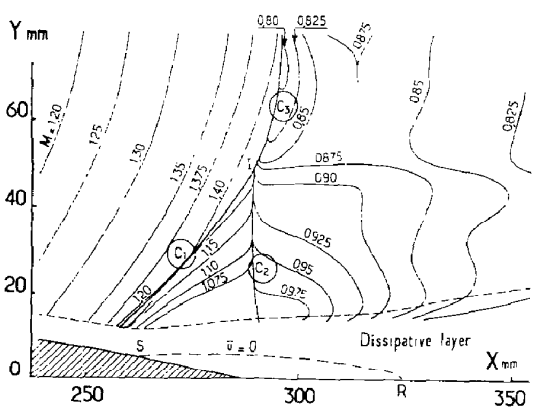

FIG. 5. Flow structure.

The initialization is done, assuming constant pressure and Mach number in the whole field, in spite of the lower wall geometry. A no-slip condition is imposed on the wall boundary. As inlet boundary conditions, the mass flow and the total enthalpy are conserved. The velocity is parallel to the walls and a characteristic relation supplies the downstream–upstream influence. At the exit boundary, the static pressure is given, whereas all other flows variables are evaluated only from the calculation domain. It was found impossible to start the calculation with the complete turbulence model. A correct initialization of the turbulence variables was very difficult to perform and the permissible time step was too small to build the mean flow efficiently. A complete calculation was done in the following way:

1. Algebraic model calculation.
2. Uncoupled turbulence field calculation.
3. Full two-equation model calculation.
4. Check of the steady state solution independence with respect to the time step value.

The first stage builds efficiently the mean field in agreement with the no-slip boundary conditions and the geometrical nozzle properties (Fig. 6).

The switching to the two-equation turbulence model shows a significant flow reorganization in and above the interaction region (Fig. 7). The shock wave changes shape and moves downstream in the inviscid part whereas the separation is enhanced in length and thickness. As the eddy viscosity is now very small in the inviscid part, the numerical upper wall boundary layer dispears in agreement with the mesh resolution.

The results, corresponding respectively to the mixing length and the two equation model, are presented on Figs. 8 to 12. Figure 8 shows the shock position for the algebraic model calculation. The shock wave is curved across the channel and

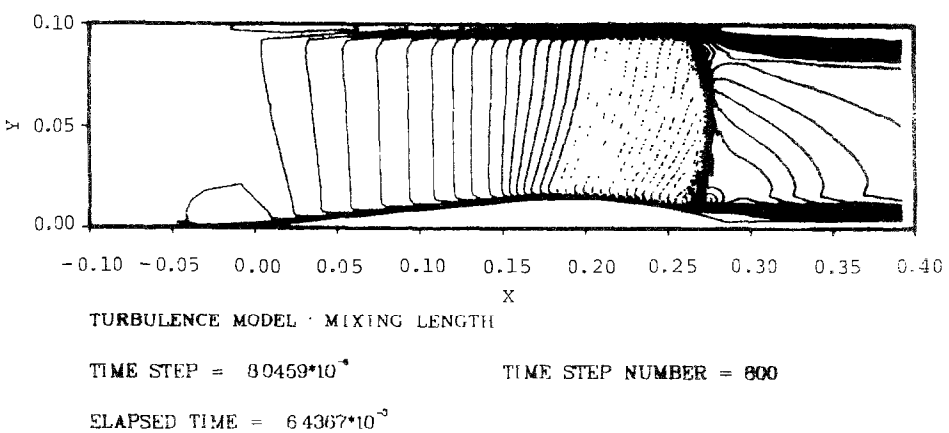

FIG. 6. Mixing length solution.

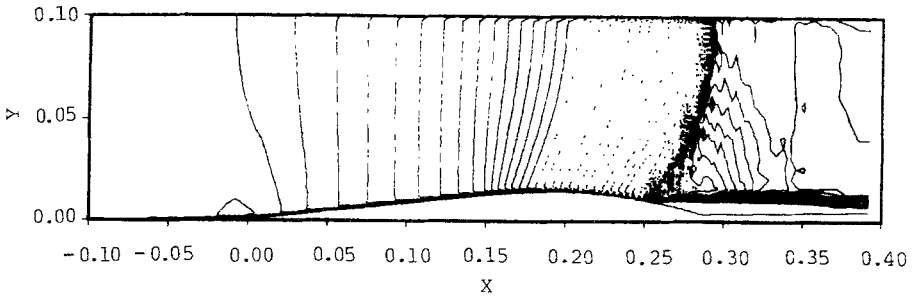

FIG. 7. *k*-epsilon solution.

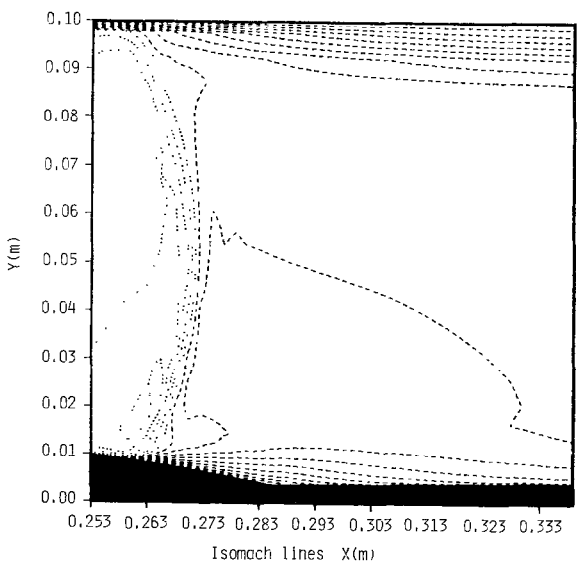

FIG. 8. Zero-order closure (algebraic model).

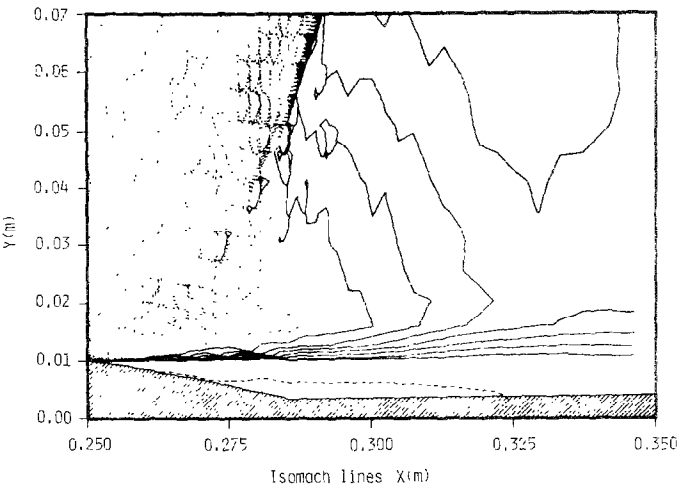

FIG. 9. Zero-order closure ($k-\varepsilon$).

located about 4cm upstream of the experimentally observed position. The separation cannot be observed, and so the expected shape of the shock wave.

Figure 9 shows a great improvement with the two equation turbulence model. The separated zone limits are correctly predicted. The weak oblique shock C_1 is well described with a large downstream supersonic zone. But the second normal shock C_2 is not predicted and the transition between the supersonic and subsonic

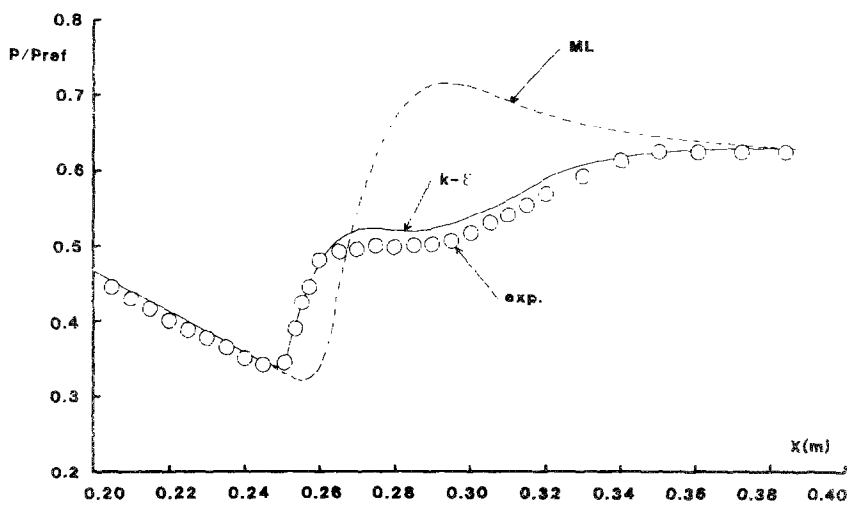

FIG. 10. Lower wall pressure.

model. In a different paper [3], the turbulence modeling effort, related to this work has been exposed and the weakness of this class of model has been explained.

Figure 10 compares the pressure distributions on the lower wall. The agreement, which is obtained with the second model is remarkably better, the plateau pressure corresponding to the separated region is well predicted. whereas the mixing length calculation does not catch this extended separation region. Nevertheless, in both cases, the pressure distributions are correctly described before and after the intraction zone.

The absence of any smoothing technique in the code allows the existence of oscillations around the shock wave, where the viscous effects are not important (Fig. 11). The decision, not to include any smoothing parameter has been taken to avoid the interferences between the turbulence model and the numerical diffusion terms. This allows also a very accurate definition of the shock wave location.

Figure 12 compares the velocity distributions with the measured values at different locations, before, inside and after the interaction region. As it could be expected from the wall pressure results, the second model provides a much better prediction but this result is not yet quite satisfactory. Indeed, an under estimation of the velocity modulus in the recirculation zone is still present and the profiles show a small defect in the transition zone between inviscid and viscous regions.

6.2. *Supersonic Interaction*

Calculations have also been performed with a second order closure model [2, 3, 4] for a supersonic flat plate boundary layer and a 12-degree compression–expansion ramp. These calculations have allowed a significant improvement in the wall turbulence anisotropy prediction, together with a better understanding of the two equation type model limits. To illustrate this, Figs. 13–17 show the results for the 12 degree deviation. The free stream Mach number is equal to 3 and the Reynolds number, based on the momentum thickness is 10,000. Figure 13 show the mean flow features. The free stream flow follows the Rankine–Hugoniot jump conditions and the Prandtl–Meyer expansion rules. A more interesting observation regards the pressure gradient influence on the turbulence anisotropy (Figs. 14–17).

The k and $\widetilde{u''^2}$ curves are quite similar except in level. The pressure gradients induce the same effects on these two quantities, i.e., increase in compression and decrease in expansion. Differently, the second normal component $\widetilde{v''^2}$ is marginally affected by the pressure gradients. But this last component is a driving quantity for all the transverse diffusion mechanisms. As all the two equation turbulence models use a part of k to simulate the diffusion coefficient, a correct prediction is hopeless, due to the fundamentally different behaviour of k and $\widetilde{v''^2}$. The Wilcos–Traci [10] model interprets k as $\widetilde{v''^2}$, but doing so, it looses all information about the k level and the definition of the turbulence scales.

It must be noticed that the turbulence increase due to the pressure gradient

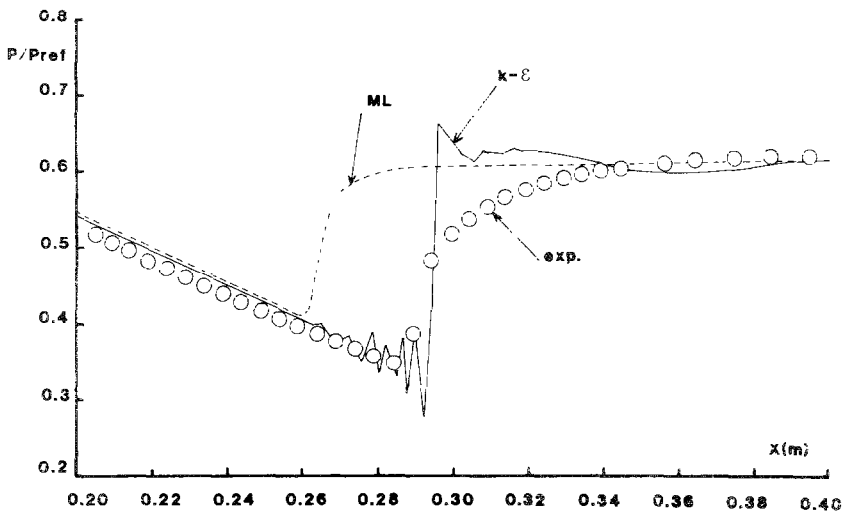

FIG. 11. Upper wall pressure.

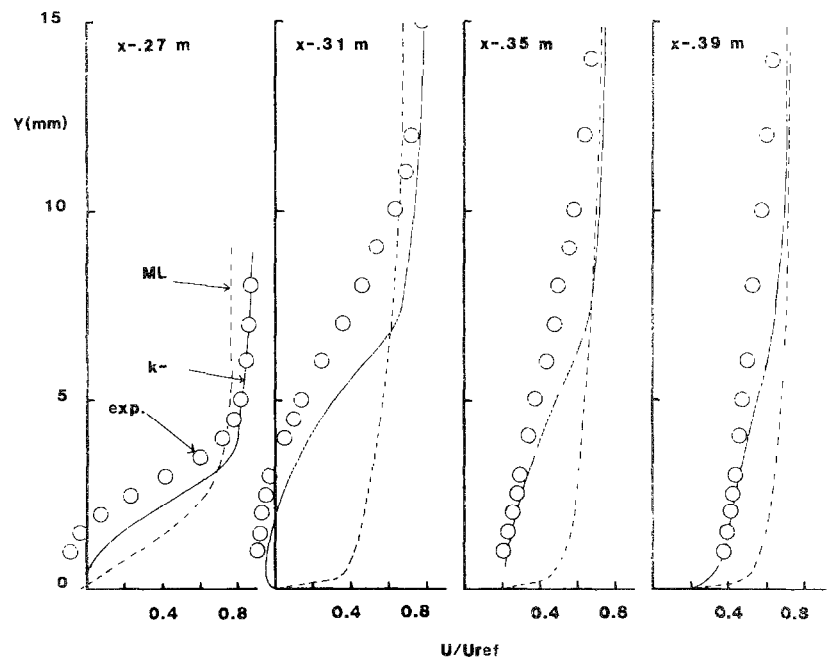

FIG. 12. Velocity profiles.

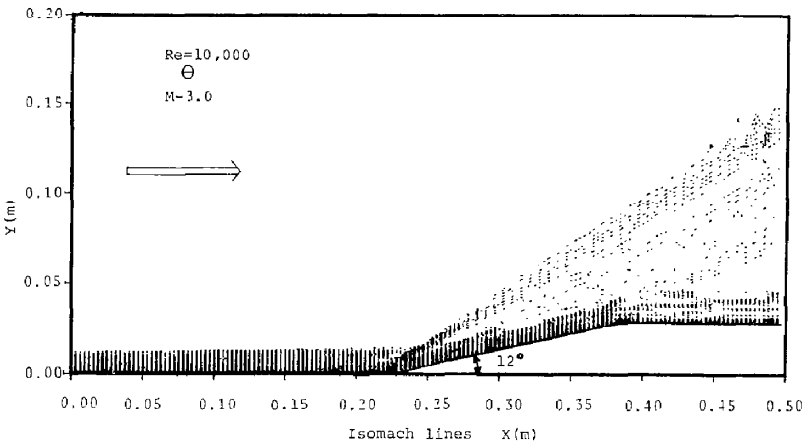

FIG. 13. Second-order closure.

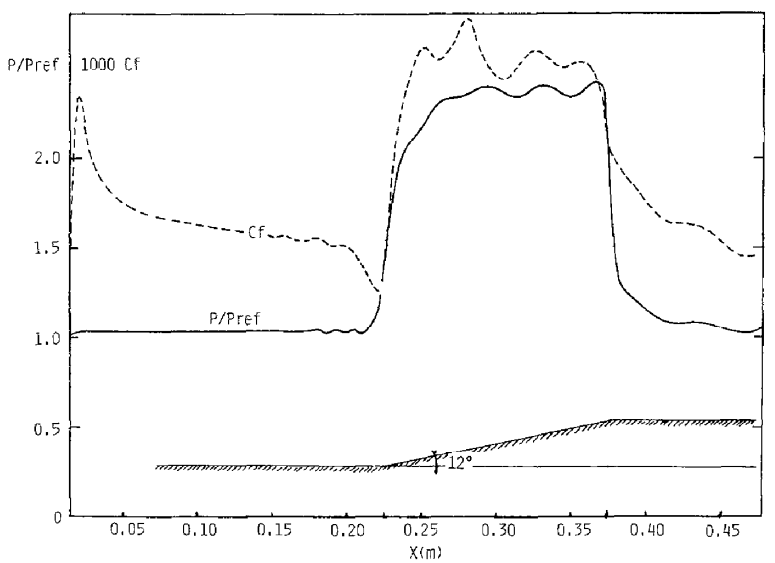

FIG. 14. Calculated skin friction and pressure distributions.

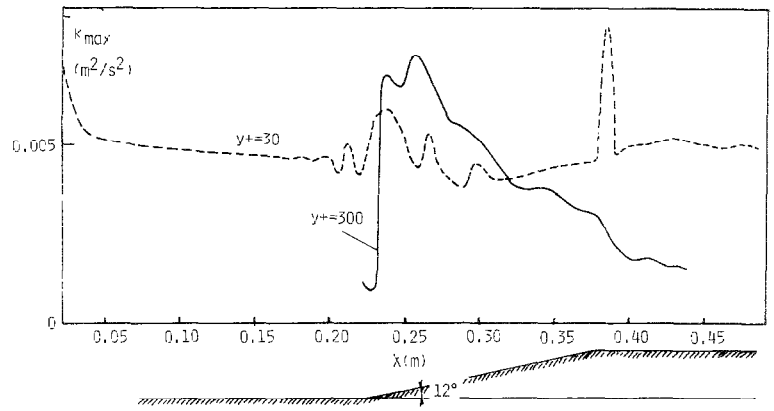

FIG. 15. Turbulent energy distribution.

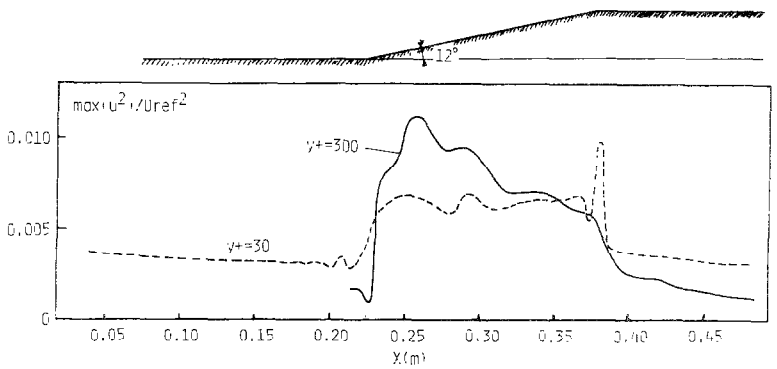

FIG. 16. Turbulent energy distribution.

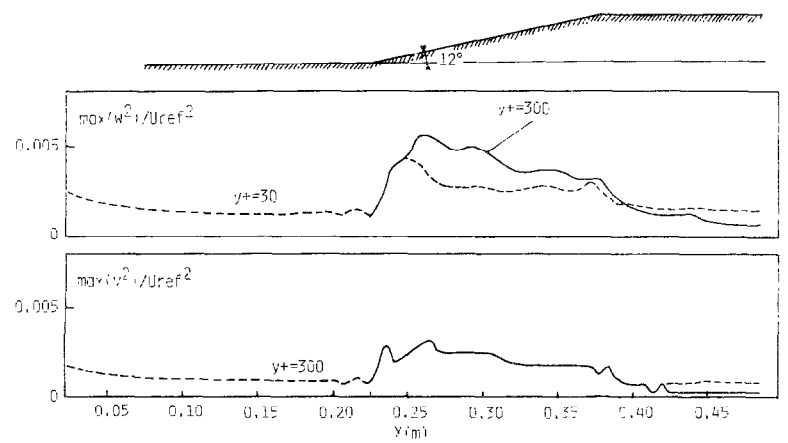

FIG. 17. Turbulent energy distribution.

occurs at $y+ = 300$, whereas the turbulence energy peak in an equilibrium boundary layer is located at $y+ = 30$. This remark holds also for the first and third normal components, but not for the second one for which the maximum is already located at $y+ = 300$.

7. Conclusion

Different turbulence models have been introduced in a Navier–Stokes solver. The different coupling features between the density-weighted averaged Navier–Stokes equations and the transport equations for the turbulent quantities have been examined. The justification of this coupling is provided by the requisite closure problem considering the various compressible flow energy transfer mechanisms between the mean and turbulent motions.

Since in the implicit operator the jacobian matrices are diagonalized to avoid the costly block tri-diagonal matrix inversion algorithm, the coupling yields some additive terms in the diagonalization matrices. Furthermore, the source term treatment is done by a third factorization which avoids the prior knowledge of the analytical content of the RHS terms. With all these characteristics, the prediction of the strong shock-boundary layer interaction in a 2-dimensional transonic nozzle has been possible.

The results are better with a two equation turbulence model than with a classical algebraic formulation. Nevertheless, the turbulence quantities are still badly described. Further calculations for a supersonic 12 degree compression–expansion flow show promising results with a second-order closure turbulence model. The weaknesses of the gradient flux approximation are particularly pointed out and the interest of this closure level extension to complex interacting flows is shown.

Acknowledgments

The material for this article has been gained through numerous discussions and exchanges with R. W. MacCormack, M. W. Rubesin, J. R. Viegas, T. J. Coakley. and W. Kollmann. This work has been supported by NASA Ames Research Center through Grant NCC2-186. Part of the computing time has been provided by the French CCVR (Centre de Calcul Vectoriel pour la Recherche).

References

1. R. W. Mac Cormack, *AIAA* paper 81-0110.
2. D. Vandromme, thèse de Doctorat d'État, Université de Lille, France, 1983 (unpublished).
3. D. Vandromme, H. Haminh, J. R. Viegas, M. W. Rubesin, and W. Kollmann, in *Proceedings of the 4th Symposium on Turbulent Shear Flows, Karlsruhe, West Germany, 1983.*
4. D. Vandromme and H. Haminh, *Von Karman Institute Lecture Lecture Serie On Computational Fluid Dynamics*, (Rhode St. Genese, Belgium, 1983).

5. W. G. VINCENTI AND C. H. KRUGER, *Introduction to Physical Gas Dynamics*. (Krieger, Huntington, New York, 1977).
6. R. W. MAC CORKMACK, *Transonic, Shock, and Multidimensional Flows: Advances in Scientific Computing* (Academic Press, New York, 1982).
7. J. R. VIEGAS. NASA-Ames Research Center, private communication, 1983.
8. J. M. DELERY AND LE DIUZET, ONERA-TP-1979-146, Paris, France, 1979 (unpublished).
9. T. CEBECI, A. M. O. SMITH, AND S. G. MOSINSKI, *AIAA J.* **8**, 1974 (1970).
10. D. C. WILCOX AND R. M. TRACI, AIAA paper 76–351, 1976 (unpublished).
11. B. S. BALDWIN, R. W. MAC CORMACK, AND G. S. DEIWERT, AGARD Lecture Serie Vol. 73, 1975.
12. J. R. VIEGAS AND T. J. COAKLEY, AIAA paper 77-44, 1977 (unpublished).
13. M. W. RUBESIN, NASA TM X-73, 1976, p. 128 (unpublished).
14. R. W. MAC CORMACK, NASA TM X-73, (1976), p. 129 (unpublished).
15. J. R. VIEGAS AND C. C. HORSTMAN, AIAA paper 67-1165, 1978 (unpublished).
16. T. J. COAKLEY AND J. R. VIEGAS, in *Proceedings of the 1st Symposium on Turbulent Shear Flows*, Penn State Univ., 1977 (unpublished).
17. T. J. COAKLEY, J. R. VIEGAS, AND C. C. HORSTMAN, AIAA paper 77-692, 1977 (unpublished).